



**HAL**  
open science

## Improving Cycling Stability of the Lithium Anode by a Spin-Coated High-Purity Li(3)PS(4) Artificial SEI Layer

Hongjiao Wang, Lilin Wu, Bai Xue, Fang Wang, Zhongkuan Luo, Xianghua Zhang, Laurent Calvez, Ping Fan, Bo Fan

► **To cite this version:**

Hongjiao Wang, Lilin Wu, Bai Xue, Fang Wang, Zhongkuan Luo, et al.. Improving Cycling Stability of the Lithium Anode by a Spin-Coated High-Purity Li(3)PS(4) Artificial SEI Layer. ACS Applied Materials & Interfaces, 2022, 14 (13), pp.15214-15224. 10.1021/acsami.1c25224 . hal-03632073

**HAL Id: hal-03632073**

**<https://hal.science/hal-03632073>**

Submitted on 11 Apr 2023

**HAL** is a multi-disciplinary open access archive for the deposit and dissemination of scientific research documents, whether they are published or not. The documents may come from teaching and research institutions in France or abroad, or from public or private research centers.

L'archive ouverte pluridisciplinaire **HAL**, est destinée au dépôt et à la diffusion de documents scientifiques de niveau recherche, publiés ou non, émanant des établissements d'enseignement et de recherche français ou étrangers, des laboratoires publics ou privés.

# Improving cycling stability of lithium anode by spin-coated high-purity $\text{Li}_3\text{PS}_4$ artificial SEI layer

*Hongjiao Wang<sup>a, b</sup>, Lilin Wu<sup>c</sup>, Bai Xue<sup>a</sup>, Fang Wang<sup>c</sup>, Zhongkuan Luo<sup>c</sup>, Xianghua Zhang<sup>b</sup>, Laurent Calvez<sup>b</sup>, Ping Fan<sup>\*a</sup>, Bo Fan<sup>\*a</sup>*

## AUTHOR ADDRESS

a. Shenzhen Key Laboratory of Advanced Thin Films and Applications, College of Physics and Optoelectronic Engineering, Shenzhen University, Shenzhen 518060, Guangdong, China.

b. Laboratory of Glasses and Ceramics, Institute of Chemical Science, University of Rennes 1, Rennes 35042.

c. College of Chemistry and Environmental Engineering, Shenzhen University, Shenzhen 518060, Guangdong, China.

† \*Corresponding author E-mail addresses: fanping@szu.edu.cn (Ping Fan), fanb07@hotmail.com (Bo Fan).

## Highlight

1. The high-purity  $\text{Li}_3\text{PS}_4$  SEI prepared by spin-coating for the first time has a controllable nanometer thickness and good electrical conductivity.

2.  $\text{Li}_3\text{PS}_4$ -protected Li can be stably cycled for 800 h at  $1 \text{ mA cm}^{-2}$  and  $1 \text{ mAh cm}^{-2}$ .
3.  $\text{Li}_3\text{PS}_4$ -protected Li improves capacity retention and rate performance of batteries.

ABSTRACT: Controlling the composition and microstructure of the solid electrolyte interphase (SEI) layer is critical to improving the cycling stability of the high-energy-density lithium-metal electrode. It is a quite tricky task to control the properties of the SEI layer which is conventionally formed by the chemical reactions between a Li metal and the additives. Herein, we develop a new route to synthesize a lithium-compatible sol of the sulfide electrolyte  $\text{Li}_3\text{PS}_4$ , so that a  $\text{Li}_3\text{PS}_4$  artificial SEI layer with a controllable nanoscale thickness and high phase purity can be prepared by spin-coating. The layer stabilizes the lithium/electrolyte interface by homogenizing the Li-ion flux, preventing the parasitic reactions, and alleviating concentration polarization. Consequently, a symmetrical cell with the  $\text{Li}_3\text{PS}_4$ -modified lithium electrodes can achieve stable lithium plating/stripping for 800 h at a current density of  $1 \text{ mA cm}^{-2}$ . The Li-S batteries assembled with the  $\text{Li}_3\text{PS}_4$ -protected Li anodes show better capacity retention than their bare Li counterparts, whose average decay rate from the 240<sup>th</sup> cycle to the 800<sup>th</sup> cycle is only 0.004%/cycle. In addition, the  $\text{Li}_3\text{PS}_4$  layer improves the rate

capacity of the batteries, significantly enhancing the capacity from 175 mAh g<sup>-1</sup> to 682 mAh g<sup>-1</sup> at a 2 C rate. The spin-coated Li<sub>3</sub>PS<sub>4</sub> artificial SEI layer provides a new strategy to develop high-performance Li metal batteries.

**KEYWORDS:** *lithium anode, Li<sub>3</sub>PS<sub>4</sub>, spin-coated, artificial SEI layer, sulfide solid electrolyte, cycle stability, lithium–metal batteries.*

## **INTRODUCTION**

Lithium (Li) has received widespread attention because of its high theoretical capacity of 3860 mAh g<sup>-1</sup> and low electrochemical potential (−3.04 V vs standard hydrogen electrode).<sup>1-4</sup> However, there are still some problems that hinder the application of Li anode. The unstable solid electrolyte interphase (SEI) formed on the lithium-metal electrode is one of the important issues.<sup>5, 6</sup> Owing to the extremely low redox potential, the Li electrode inevitably reacts with the electrolyte to form the heterogeneous SEI. Usually, the SEI is fragile and suffers a vicious cycle of formation, rupture and reformation. This will not only lead to the formation of dead Li and electrode powdering, but also aggravates the uneven deposition of Li which induces dendrite growth.<sup>7-9</sup> Unstable SEI will cause a sharp drop in battery performance. Then, electrolyte additives are widely used to stabilize the SEI. The electrolyte additives change the composition of the SEI by participating in the formation reaction of the SEI.

It is revealed that the additives such as lithium bisfluorosulfonimide (LiFSI)<sup>10</sup>, lithium hexafluorophosphate (LiPF<sub>6</sub>)<sup>11</sup>, lithium nitrate (LiNO<sub>3</sub>)<sup>12</sup>, and polysulfide<sup>13</sup> can increase the inorganic contents such as LiF, Li<sub>3</sub>N and Li<sub>2</sub>S in the SEI, improving its ionic conductivity and toughness. This promotes the stable cycling of the Li electrode. The SEI modified by the electrolyte additives still exhibits a multi-phase heterogeneous mosaic structure, which harms the deposition uniformity of Li and the toughness against the stress caused by the volume change of the Li anode.<sup>14-18</sup> Moreover, with the continuous consumption of the additives, the protection ability of the modified SEI is gradually weakened during the long-term cycling.

Recently, the artificial SEIs are constructed on the surface of the Li anode before battery assembling, whose microstructure can be better controlled in comparison with the additive-modified SEI.<sup>19, 20</sup> Li et al.<sup>21</sup> reported that an artificial SEI layer of Li<sub>3</sub>PO<sub>4</sub> could be formed by the reaction of polyphosphoric acid with lithium, which suppressed parasitic reactions between lithium anode and electrolyte. More attention has been appealed to the Li<sub>3</sub>PS<sub>4</sub>-based SEI layers, viewing that the high ionic conductivity of the SEI layer improves the lithium deposition/plating homogeneity. Pang et al.<sup>22</sup> used Li<sub>2</sub>S<sub>6</sub> and P<sub>2</sub>S<sub>5</sub> as additives which in-vivo reacted with Li anode to form Li<sub>3</sub>PS<sub>4</sub> SEI layer. The strategy improved the cycle performance of lithium symmetrical cells and inhibited

the formation of lithium dendrites. The thickness and composition of the in-vivo formed  $\text{Li}_3\text{PS}_4$  SEI layer were somehow difficult to control due to the complex reaction condition within the battery, which resulted in a relatively large hysteresis voltage of lithium symmetrical cells during long-term cycling. Liang et al.<sup>23</sup> reacted  $\text{P}_4\text{S}_{16}$  and lithium to prepare  $\text{Li}_3\text{PS}_4$ -protected Li anodes. Benefitting from the good controllability of the reaction out of the batteries, the thickness of the protective layer could be controlled to nanoscale so that excellent cycling performance in lithium symmetrical cells and Li-S batteries were obtained. These studies show that high phase purity and nanoscale thickness are essential to achieve good Li-protection ability of the  $\text{Li}_3\text{PS}_4$ -based SEI layer.

Since the complexity of the reaction between lithium and the phosphor-sulfur compounds, the thickness and phase purity of these ex-situ  $\text{Li}_3\text{PS}_4$  SEI layers are still difficult to control.<sup>24</sup> Here, a new strategy is proposed to prepare a nanoscale  $\text{Li}_3\text{PS}_4$  artificial SEI layer with good phase purity for lithium anode. This strategy includes the synthesis of a lithium-compatible  $\text{Li}_3\text{PS}_4$  sol and a following spin-coating of the sol to form a 650-nm thick  $\text{Li}_3\text{PS}_4$  layer on the Li electrode. With the protection of the  $\text{Li}_3\text{PS}_4$  layer, the lithium symmetrical cells can stably cycle for 800 h under  $1 \text{ mA cm}^{-2}$  with a low hysteresis voltage of about 25 mV, showing great advantages over the cells with

the bare lithium electrodes, whose stable cycling lasts only 200 h. The improved electrochemical performance of the  $\text{Li}_3\text{PS}_4$ -protected Li electrode is also demonstrated in Li-S batteries and Li- $\text{LiFePO}_4$  (LFP) batteries. At 1 C rate, the Li-S battery with the protected Li anode shows a quite low average capacity decay rate of 0.004%/cycle from 240<sup>th</sup> cycle to 800<sup>th</sup> cycle. For the Li-LFP battery, the  $\text{Li}_3\text{PS}_4$  artificial SEI layer guarantees stable operation of the batteries over 145 cycles, while the battery with the bare Li anode fails in 100 cycles.

## **EXPERIMENTAL SECTION**

### **Preparation of $\text{Li}_3\text{PS}_4$ sol**

The chemicals used were sulfur powder (99.5%, Alfa Aesar), tetrahydrofuran ( $\geq 99.5\%$ , Aladdin),  $\text{LiEt}_3\text{BH}$  (1 M, Innochem),  $\text{Li}_2\text{S}$  (99.9%, Alfa Aesar),  $\text{P}_2\text{S}_5$  (99%, Aladdin), poly(1,1-difluoroethylene) (Macklin), N-methyl-2-pyrrolidone (99.9%, Aladdin), 1.0 M  $\text{LiN}(\text{CF}_3\text{SO}_2)_2$  (LiTFSI) in 1,3-dioxolane/dimethyl ether (DOL/DME, 50–50 vol.%) with 1.0 wt.%  $\text{LiNO}_3$  and 1.0 M  $\text{LiPF}_6$  in ethylene carbonate/diethyl carbonate (EC/DEC, 50–50 vol.%) were used as electrolytes, which were purchased from Do Do Chem. All the chemicals were used as is, without further purification.

Dual-precursor liquid phase synthesis method was applied to prepare  $\text{Li}_3\text{PS}_4$  sol. First, 4 mmol sulfur powder was added into 8 mL of tetrahydrofuran (THF) solution

containing  $\text{LiEt}_3\text{BH}$ . After stirring for 3 h, the  $\text{Li}_2\text{S}$  sol was obtained. The sol was further purified by centrifugation and then redispersed in THF. Second, a certain amount of  $\text{Li}_2\text{S}$  and  $\text{P}_2\text{S}_5$  (molar ratio 1:1) was added into 3 mL of THF, and stirred for 40 min to obtain a  $\text{Li}_2\text{S}\cdot\text{P}_2\text{S}_5$  solution. Finally, the  $\text{Li}_2\text{S}\cdot\text{P}_2\text{S}_5$  solution was added to the  $\text{Li}_2\text{S}$  sol to get the  $\text{Li}_3\text{PS}_4$  sol, and the molar ratio of  $\text{Li}_2\text{S}$  and  $\text{P}_2\text{S}_5$  was 3:1. The concentration of the  $\text{Li}_3\text{PS}_4$  sol was controlled to be 0.1, 0.08, 0.06, 0.04 and 0.02 M, respectively, by adjusting the concentration of the two precursors. All the operations were conducted in an argon-filled glovebox ( $\text{O}_2 < 0.5$  ppm,  $\text{H}_2\text{O} < 0.5$  ppm).

### **Preparation of $\text{Li}_3\text{PS}_4$ artificial SEI layer**

The  $\text{Li}_3\text{PS}_4$  artificial SEI layer was prepared by spin-coating. First, 100  $\mu\text{L}$  of the  $\text{Li}_3\text{PS}_4$  sol was dropped on the Li sheet. Then the Li sheet spun at 4000 rpm to spread the sol. After drying at room temperature for 2 min, a thin layer of  $\text{Li}_3\text{PS}_4$  formed on the Li sheet. This operation could be repeated several times to achieve the desired thickness. The  $\text{Li}_3\text{PS}_4$  sols with different concentrations (0.1, 0.08, 0.06, 0.04 and 0.02 M) were used for spin-coating, so that the quality of the  $\text{Li}_3\text{PS}_4$  artificial SEI layer can be optimized. The obtained  $\text{Li}_3\text{PS}_4$ -protected lithium electrode is denoted as Li/LPS-0.1, Li/LPS-0.08, Li/LPS-0.06, Li/LPS-0.04 and Li/LPS-0.02 respectively. The spin-coating was conducted in an argon-filled glovebox ( $\text{O}_2 < 0.5$  ppm,  $\text{H}_2\text{O} < 0.5$  ppm).

## Material Characterizations

The morphology of the samples was characterized by a field-emission scanning electron microscope (SEM, SU8010, Hitachi Inc., Japan). An energy-dispersive X-ray microanalyzer (EDS) integrated with the scanning electron microscope was used to characterize the composition of the samples. The phase structure of the samples was characterized by X-ray diffraction (XRD, D8 Advance, Bruker AXS GmbH, Germany). Raman spectra were recorded by a Raman spectrometer (in Via, Renishaw Inc., UK) with a 532-nm diode-pumped solid-state laser as the excitation source. The samples for XRD and Raman spectroscopy were sealed by a polyimide film to protect them from air humidity. The interfacial chemistry of the Li electrodes was analyzed by X-ray photoelectron spectroscopy (XPS, ESCALAB 250Xi, Thermo Scientific Inc., US) with Al  $K_{\alpha}$ -radiation.

## Electrochemical Measurements

Lithium symmetrical cells were assembled with Li/LPS or bare Li as the electrodes. A Celgard 2300 membrane was used as the separator. 1 M LiN(CF<sub>3</sub>SO<sub>2</sub>)<sub>2</sub> (LiTFSI) in 1,3-dioxolane/dimethyl ether (DOL/DME, 50–50 vol.%) with 1 wt.% LiNO<sub>3</sub> additive was used as the electrolyte. The components were packaged into CR2032 coin-type cells. Lithium plating/stripping cycles were monitored by a battery tester (CT2001,

Wuhan Land Electronics Co. Ltd., China). The impedance spectra of the cells were recorded by an electrochemical workstation (CHI660E, CH Instruments Ins., China).

The CR2032 coin-type Li-S batteries were assembled using S@C electrode as the cathode, Li<sub>3</sub>PS<sub>4</sub>-protected Li or bare Li as the anode, Celgard 2300 membrane as the separator and 1 M LiTFSI dissolved in DOL/DME (50–50 vol.%) with 1 wt.% LiNO<sub>3</sub> as the electrolyte. The S@C electrode was prepared as follows: First, the S@C composite was prepared by vacuum-heating the premixed sulfur and ketjen black (7:3) at 155°C for 12 h. Then a slurry of S@C, poly(1,1-difluoroethylene), and acetylene black with a mass ratio of 8:1:1 was mixed in N-methyl-2-pyrrolidone (NMP). The slurry was blade-coated onto an aluminum foil. After drying in an oven at 60°C for 12 h, the aluminum foil was cut into Ø13-mm discs. The sulfur loading of the S@C electrode was 0.9–1.2 mg cm<sup>-2</sup>. Galvanostatic charge/discharge cycles of the Li-S batteries were conducted with a voltage range of 1.6–2.7 V.

The CR2032 coin-type Li-LFP batteries were assembled using LFP electrode as the cathode, Li<sub>3</sub>PS<sub>4</sub>-protected Li or bare Li as the anode, Celgard 2300 membrane as the separator and 1.0 M LiPF<sub>6</sub> in ethylene carbonate/diethyl carbonate (EC/DEC, 50–50 vol.%) as the electrolyte. Commercial LFP (Guangdong Card New Energy

Technology Co. Ltd, China) electrode was used in this study. The active material loading was  $11.5 \text{ mg cm}^{-2}$ . The voltage cutoffs of the batteries were 2.10 and 4.20 V.

## RESULTS AND DISCUSSION

### Characterization of $\text{Li}_3\text{PS}_4$ artificial SEI layer

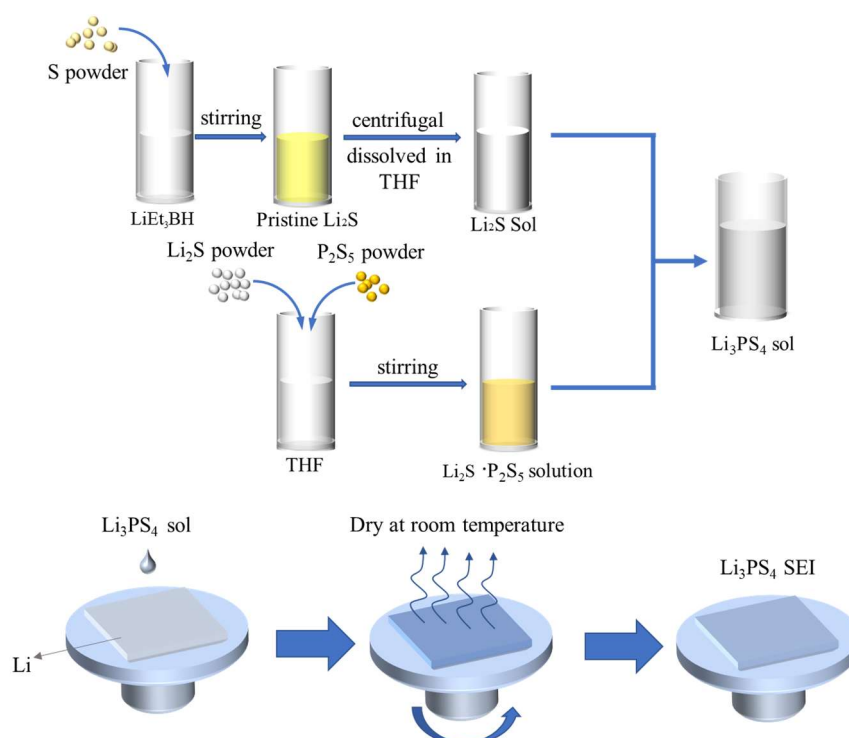
Traditional liquid-phase synthesis method by adding a stoichiometric ratio of  $\text{Li}_2\text{S}$  and  $\text{P}_2\text{S}_5$  in THF can only produce  $\text{Li}_3\text{PS}_4$  suspension with micron-sized particles.<sup>25</sup> This  $\text{Li}_3\text{PS}_4$  suspension cannot form continuous film by spin-coating owing to the large particles size. Therefore, a novel synthesis route of nano-sized  $\text{Li}_3\text{PS}_4$  has been developed here. The preparation of the  $\text{Li}_3\text{PS}_4$  artificial SEI layer is described in Schematic 1. This work uses the reaction of  $\text{LiEt}_3\text{BH}$  and S to prepare a THF sol containing  $\text{Li}_2\text{S}$  nanoparticles (Figure S1a). Then, a THF solution containing  $\text{P}_2\text{S}_5 \cdot \text{Li}_2\text{S}$  is prepared, and it is added dropwise to the  $\text{Li}_2\text{S}$  sol to trigger the reaction  $2\text{Li}_2\text{S} + \text{P}_2\text{S}_5 \cdot \text{Li}_2\text{S} = 2\text{Li}_3\text{PS}_4$ . Benefiting from the nanoscale particle size of  $\text{Li}_2\text{S}$ , the reaction completes within 1 h, resulting in a transparent sol containing  $\text{Li}_3\text{PS}_4$  nanoparticles (Figures S1b, c). Finally, the sol was spin-coated onto the Li sheet and dried at room temperature to form the artificial SEI layer.

The phase structure of the as-prepared high-purity  $\text{Li}_3\text{PS}_4$  is identified by XRD (Figure 1a). After drying the sol at  $60^\circ\text{C}$ , the diffraction peaks attributed to

$\text{Li}_3\text{PS}_4 \cdot 3\text{THF}$  can be clearly seen.<sup>25</sup> When the sample is heat-treated at  $140^\circ\text{C}$ , the signal of  $\text{Li}_3\text{PS}_4 \cdot 3\text{THF}$  disappears and that of  $\beta\text{-Li}_3\text{PS}_4$  appears. This indicates that the as-prepared  $\text{Li}_3\text{PS}_4$  in the sol is solvated by THF, while the de-solvation can be achieved by  $140^\circ\text{C}$  heat treatment. The conclusion is further supported by the Raman results in Figures 1b, c. A single peak at about  $423\text{ cm}^{-1}$  dominates the low-wavenumber region of the Raman spectra, which is assigned to  $\text{PS}_4^{3-}$ .<sup>26</sup> The slight shift of the peak to  $421\text{ cm}^{-1}$  is observed in the  $60^\circ\text{C}$ -dried sample, associated with the solvation effect of THF. The absence of the signals of  $\text{P}_2\text{S}_6^{2-}$  ( $380\text{ cm}^{-1}$ ) and  $\text{P}_2\text{S}_7^{4-}$  ( $410\text{ cm}^{-1}$ ) excludes the impurity such as  $\text{Li}_2\text{P}_2\text{S}_6$  and  $\text{Li}_4\text{P}_2\text{S}_7$ .<sup>22, 27</sup> In the high-wavenumber region, C-H stretching signal from THF ( $2900\text{--}3000\text{ cm}^{-1}$ ) is observed in the  $60^\circ\text{C}$ -dried sample, which disappears after  $140^\circ\text{C}$  heat treatment, confirming the de-solvation of THF at  $140^\circ\text{C}$ .

At low magnification, the top-view SEM image of  $\text{Li}_3\text{PS}_4$ -protected Li shows a flat surface without observable graininess (Figure 1d). Comparing the smooth surface morphology of the  $\text{Li}_3\text{PS}_4$ -protected Li (Figure 1e) with the textured surface morphology of bare Li (Figure 1g) at high magnification, it can be further confirmed that the spin-coated  $\text{Li}_3\text{PS}_4$  homogeneously covers the surface of Li, forming a dense and smooth layer. The thickness of the protective layer is measured from its cross-

sectional SEM image in Figure 1f, and it turned out to be about 650 nm. Then, in Figure 1h, the elemental analysis of the  $\text{Li}_3\text{PS}_4$  film is carried out. As shown by the EDS spectrum in Figure S2, evident signals of P and S are observed, which come from the  $\text{Li}_3\text{PS}_4$  artificial SEI layer. The O element may come from THF (Figure 1i). Quantitative analysis results listed in Table S1 reveal that the atomic ratio of P and S elements is about 1:3.4, closing to the stoichiometric ratio of  $\text{Li}_3\text{PS}_4$ . The homogeneous distribution of S and P on the lithium surface can be seen in the EDS mapping (Figures 1j, k), further confirming that the lithium surface is evenly covered by the  $\text{Li}_3\text{PS}_4$  artificial SEI layer.



Schematic 1. Synthesis route of the  $\text{Li}_3\text{PS}_4$  sol and the preparation of the  $\text{Li}_3\text{PS}_4$  artificial SEI layer on Li by a spin-coating process.

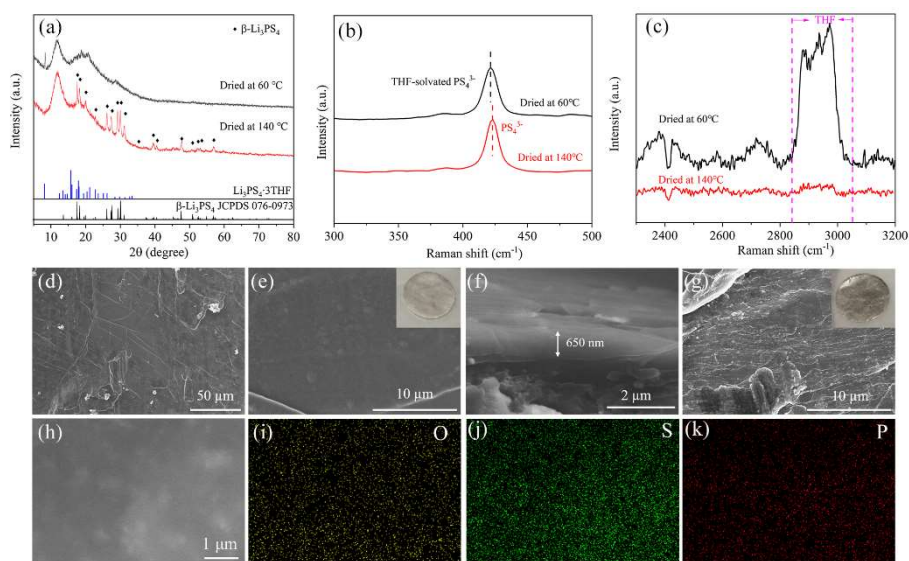


Figure 1. (a) XRD patterns of  $\text{Li}_3\text{PS}_4$  prepared at different drying temperatures. (b, c) Raman spectra of  $\text{Li}_3\text{PS}_4$  prepared at different drying temperatures in the low-wavenumber region and high-wavenumber region, respectively. SEM images of the  $\text{Li}_3\text{PS}_4$ -modified Li (Li/LPS-0.06M) and bare Li. (d, e) Top-view image and (f) cross-sectional image of Li/LPS-0.06M. (g) Top-view image of bare Li. (h) EDS mapping of (i) oxygen, (j) sulfur and (k) phosphorus of the surface of Li/LPS-0.06M.

## Lithium symmetrical cell test

The Li symmetrical cells are assembled with the bare Li electrode and the Li/LPS-0.06M electrode. Their lithium plating/stripping performance is compared. Here we focus the discussion on the LPS-0.06M electrode. While the  $\text{Li}_3\text{PS}_4$  layer prepared with other concentrations of the precursor sol exhibit considerable Li protective ability (Figures S3–S10), the optimized Li/LPS-0.06M electrode has the most compact protective layer and shows the best cycling stability in the symmetrical cells.

The as-assembled cells firstly stand for 24 h, during which the evolution of their electrochemical impedance spectra (EIS) is monitored (Figures 2a, b). The initial interfacial resistance of the Li/LPS-0.06M symmetrical cell is 25  $\Omega$ , slightly greater than 13  $\Omega$  of the bare Li symmetrical cell. This additional resistance comes from the Li<sub>3</sub>PS<sub>4</sub> layer. With the standing time increasing, the interfacial resistance of the bare Li symmetrical cell increases significantly. This reflects that the SEI layer grows continuously owing to the parasitic reactions between the Li electrode and the electrolyte.<sup>28, 29</sup> In contrast, the interfacial resistance of the Li/LPS-0.06M symmetrical cell increases slowly, and even decreases in 15–24 h. The stable interfacial resistance benefits from the suppression of the side reactions by the Li<sub>3</sub>PS<sub>4</sub> protective layer.

The lithium plating/stripping voltage profiles of the symmetrical cells at a current density of 1 mA cm<sup>-2</sup> and a capacity of 1 mAh cm<sup>-2</sup> are presented in Figure 2c. The initial voltage of the Li/LPS-0.06M symmetrical cell is -0.062 V, which is smaller than -0.080 V of the bare Li symmetrical cell. This is due to the larger interfacial resistance of the bare Li electrode. Once the cycling starts, the hysteresis voltage of both cells decreases due to the activation of lithium-ion-conduction in the SEI layers.<sup>30</sup> In Figure 2c, the bare Li symmetrical battery stably cycles for 200 h and then its hysteresis voltage increases rapidly. In contrast, the stable cycling of the Li/LPS-0.06M symmetrical cell

greatly extends to more than 800 h. The lithium plating/stripping at a high current density of  $3 \text{ mA cm}^{-2}$  is also tested. The voltage of the Li/LPS-0.06M symmetrical cell has been demonstrated to operate stably for 350 hours. In contrast, the voltage of the bare Li symmetric cell increased rapidly after 200 h (Figure S11).

The details of the voltage profiles of the two symmetrical cells at  $1 \text{ mA cm}^{-2}$  are compared in Figures 2d–f. During the first 20 h, both cells exhibit voltage fluctuation. This voltage fluctuation is associated with the concentration polarization of the liquid electrolyte near the lithium electrodes.<sup>31</sup> With the plating/stripping cycling continues, the voltage fluctuation of the Li/LPS-0.06M symmetrical cell gradually attenuates, while the voltage fluctuation of the bare Li symmetrical cell is still obvious, as shown by the profile during 200–220 h. Finally, the voltage of the Li/LPS-0.06M symmetrical cell keeps very stable at 480–500 h, while the hysteresis voltage of the bare Li symmetrical cell dramatically increases and becomes unstable. Compared with the fragile spontaneous SEI layer, the  $\text{Li}_3\text{PS}_4$  artificial SEI layer has better toughness and more stable morphology so that the transfer number of  $\text{Li}^+$  within the SEI layer can be effectively augmented to close unity. Consequently, concentration polarization can be alleviated by the artificial SEI layer.

Alleviating concentration polarization not only stabilizes the plating/stripping voltage, but also suppresses the pulverization of lithium electrodes and the growth of dendrites. As shown by the morphology of the lithium electrodes after 500 h cycling, the bare Li electrode shows the porous and dendritic structure (Figures 3a, b), and the pulverized layer is as thick as 122  $\mu\text{m}$  (Figure 3c). In contrast, the surface of the cycled Li/LPS-0.06M electrode is smooth (Figures 3d, e). The cross-sectional SEM image shows that the deposited lithium layer is constructed by micron-sized lithium grains and the thickness is only 26  $\mu\text{m}$  (Figure 3f). These morphological characteristics are consistent with the voltage curves in Figure 2c, that is, the dendritic structure intensifies the parasitic reaction between lithium and the electrolyte, resulting in poor morphological stability of the lithium electrode and large fluctuation of the cell voltage, while the dense structure of the LPS film promotes the homogenous plating/stripping of lithium to achieve a stable voltage platform.

To further reveal the mechanism beneath the cycling stability of the Li/LPS-0.06M electrode, the impedance of the symmetrical cell after 10 cycles is measured (Figure S12 and Table S2). The resistance of the  $\text{Li}_3\text{PS}_4$  artificial SEI layer is revealed by the high-frequency semicircle and turns to be 0.8  $\Omega$ , which is much smaller than the resistance 2.9  $\Omega$  of the spontaneously formed SEI layer on the bare Li, showing the

good ion-conduction ability of the artificial SEI layer.<sup>32</sup> It has been demonstrated previously that the ether-solvated  $\text{Li}_3\text{PS}_4$  has high ionic conductivity when contacted with ether-based liquid electrolytes.<sup>33</sup> Moreover, compared with the complex composition and microstructure of the spontaneous SEI, the microstructure of the  $\text{Li}_3\text{PS}_4$  artificial SEI layer can be effectively controlled by the spin-coating process, forming a stable lithium-ion transport pathway. The good ion-conduction ability of the SEI layer favors homogeneous  $\text{Li}^+$  flux within it, which is an important factor for the stable plating/stripping of the Li/LPS-0.06M electrode.

Besides the good ion-conduction ability which homogenizes the  $\text{Li}^+$  flux, the  $\text{Li}_3\text{PS}_4$  artificial layer effectively suppresses the parasitic reactions between the lithium electrode and the electrolyte, which is studied by XPS of the bare Li and Li/LPS-0.06M electrodes after 500 h cycling. For the Li/LPS-0.06M electrode, the S  $2p_{3/2}$  peak is near 161.4 eV is assigned as  $\text{PS}_4^{3-}$  (Figure 4a), which corresponds to the P  $2p_{3/2}$  peak at 132.9 eV in the P 2p spectrum (Figure 4b). The signals of  $\text{PS}_4^{3-}$  are absent in the S 2p and P 2p spectra of the bare Li electrode.<sup>34</sup> It can be concluded that  $\text{Li}_3\text{PS}_4$  still exists on the Li/LPS-0.06M electrode after 500 h cycling. The S  $2p_{3/2}$  peaks at 169.0 eV and 167.1 eV are attributed to  $-\text{SO}_2\text{CF}_3$  and  $-\text{SO}_2\text{CF}_2^+$ , from LiTFSI and its reduction products.<sup>22, 24, 35, 36</sup> Compared with the Li/LPS-0.06M electrode, the proportion of -

$\text{SO}_2\text{CF}_2^+$  to  $-\text{SO}_2\text{CF}_3$  has increased for the bare Li electrode, indicating that LiTFSI has been deeply reduced and decomposed. The over-reduced LiTFSI on the Li anode leads to high resistance and an unstable interface.<sup>10, 37-39</sup> In contrast, the  $\text{Li}_3\text{PS}_4$  layer can alleviate the over-reduction of LiTFSI and promote the cycle stability of the Li/LPS-0.06M symmetrical cells.

For the Li 1s spectra in Figure 4c, the signals of Li-F (56.1 eV), Li-O (55.6 eV), Li-S (54.8 eV),  $\text{ROCO}_2\text{Li}$  (54.6 eV) and Li-N (54.2 eV) are detected.<sup>19, 40</sup> The Li-F and Li-N peaks of the Li/LPS-0.06M electrode are lower than that of the bare Li electrode. Correspondingly, the N 1s and F 1s spectra of the Li/LPS-0.06M electrode also show weak intensity. It indicates that the reaction of Li with LiTFSI and  $\text{LiNO}_3$  is suppressed by the  $\text{Li}_3\text{PS}_4$  layer. As shown in Figure 4d, the N 1s peaks attributed to  $\text{TFSI}^-$  (399.0 eV) and  $\text{Li}_3\text{N}$  (397.2 eV) exist in both electrodes. The formation of  $\text{Li}_3\text{N}$  is due to the decomposition of  $\text{LiNO}_3$  and  $\text{TFSI}^-$ .<sup>36, 41, 42</sup> The F 1s spectra (Figure 4e) are predominated by the peaks attributed to  $-\text{CF}_2$  (687.5 eV) and LiF (684.8 eV).<sup>43</sup> The higher relative intensity of the  $\text{Li}_3\text{N}$  and LiF peak can be observed for the bare Li electrode, indicating that the lithium salt is reduced more deeply. From Figures 4c–e, we can conclude that compared with bare Li electrodes, Li/LPS-0.06M electrodes can

alleviate the decomposition of LiTFSI and change the component content of the SEI layer.

The  $\text{Li}_3\text{PS}_4$  artificial SEI layer protects the lithium electrode from two aspects (Schematic 2). First, the good lithium-ion conductivity and high lithium transfer number promote the homogenous plating and stripping of lithium, which alleviates the local concentration of Li-ion flux and suppresses the formation of lithium dendrites. Second, the robust artificial SEI layer provides enough mechanical strength to reduce the contact as well as the parasitic reactions between Li anode and the organic liquid electrolytes, so that a highly resistive pulverized lithium layer can keep thin. To simultaneously achieve the two aspects, the artificial layer should have a proper composition with high ion conductivity, dense microstructure to keep the robust and optimized thickness to balance the ion-conduction ability and the mechanical strength.

Benefitting from the high phase purity and well-controlled nanoscale thickness of the spin-coated  $\text{Li}_3\text{PS}_4$  layer, the lithium symmetrical cell of this work has a longer cycle life under high current densities than those with the  $\text{Li}_3\text{PS}_4$  layers generated by the direct reaction on the lithium surface (Table S3).<sup>23, 24, 35</sup> The thickness and phase structure of the  $\text{Li}_3\text{PS}_4$  SEI generated by the reaction between lithium and phosphor-sulfur compounds are difficult to control, limiting the cycling performance of the

lithium electrode at a current density higher than  $1 \text{ mA cm}^{-2}$ . For example, the SEI formed by reacting  $\text{P}_4\text{S}_{10}$  with lithium makes the lithium symmetrical cell cycles for 270 h at  $1 \text{ mA cm}^{-2}$ .<sup>24</sup> In this study, the spin-coating route of the sulfide artificial SEI layer provides an effective way to control the thickness and phase purity, and consequently, the Li/LPS-0.06M symmetrical cell can stably cycle at  $1 \text{ mA cm}^{-2}$  for 800 h with a voltage hysteresis of less than 25 mV. The protected lithium electrode can even cycle for 300 h at  $3 \text{ mA cm}^{-2}$ , which is competitive with the high-rate performance of the lithium electrodes stabilized by other strategies, such as lithiophilic coating and 3D-structured electrode.<sup>44, 45</sup>

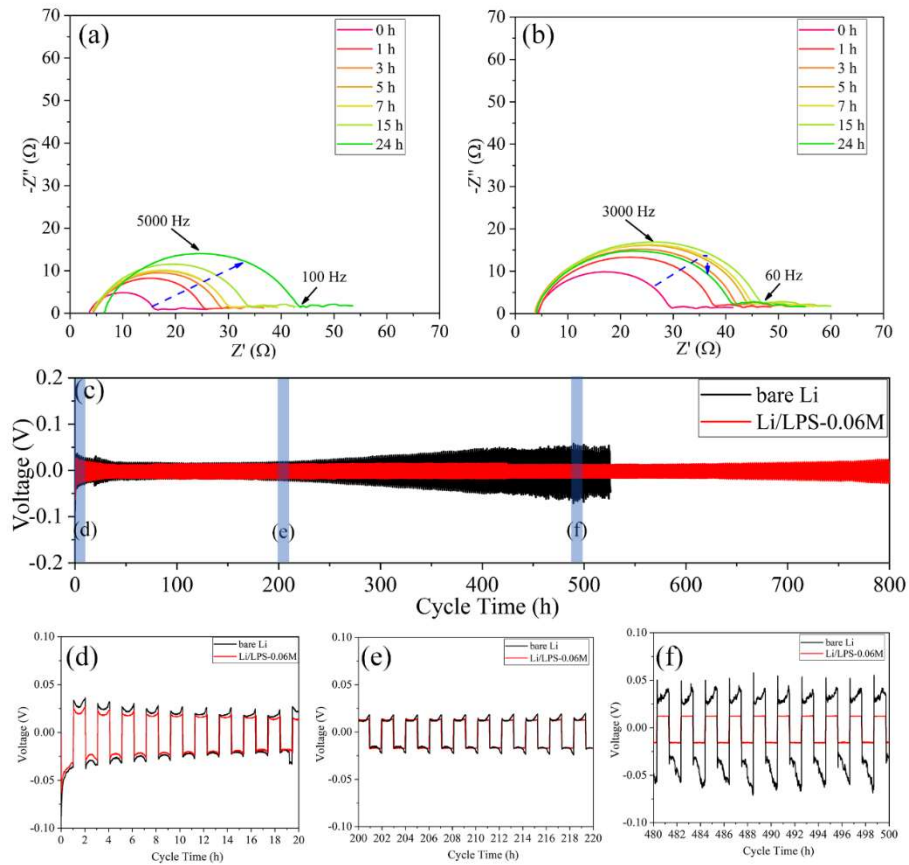


Figure 2. Evolution of the electrochemical impedance spectroscopy of (a) the bare Li symmetrical cell and (b) the Li/LPS-0.06M symmetrical cell during 24 h standing. Electrochemical characterization of the Li/LPS-0.06M and bare Li electrodes. (c) Comparison of the long cycle life of the bare Li and Li/LPS-0.06M symmetrical batteries at  $1 \text{ mA cm}^{-2}$  and  $1 \text{ mAh cm}^{-2}$ . Detailed plating/stripping voltage profiles of the Li/LPS-0.06M and bare Li symmetrical cells at different periods, (d) 0–20 h, (e) 200–220 h (f) 480–500 h.

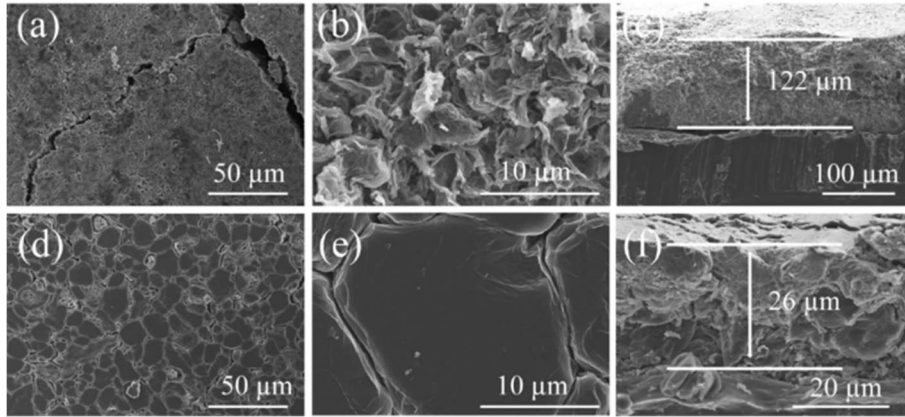


Figure 3. Morphology of the symmetrical cells with the bare Li and Li/LPS-0.06M electrodes after 500 h cycling at  $1 \text{ mA cm}^{-2}$  and  $1 \text{ mAh cm}^{-2}$ . (a, b) Top-view and (c) cross-sectional SEM images of the bare Li electrode. (d, e) Top-view and (f) cross-sectional SEM images of the Li/LPS-0.06M electrode.

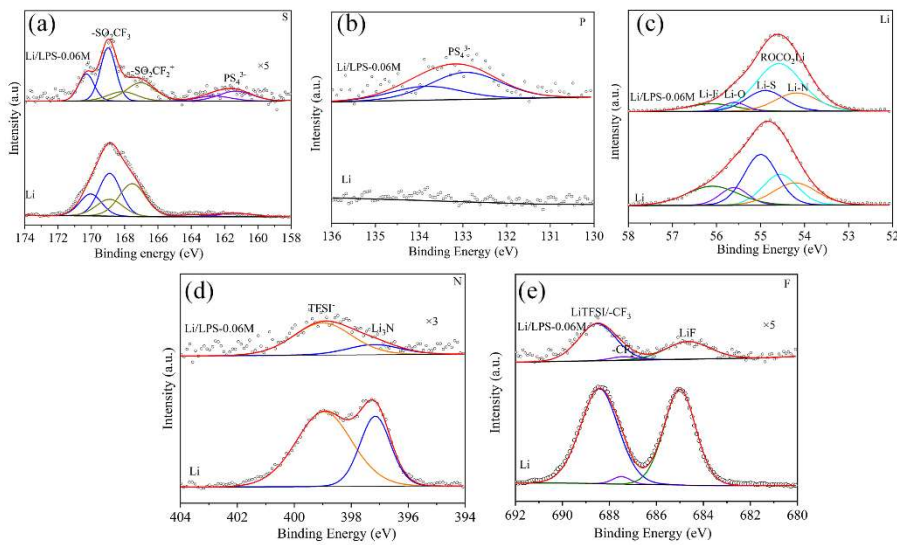
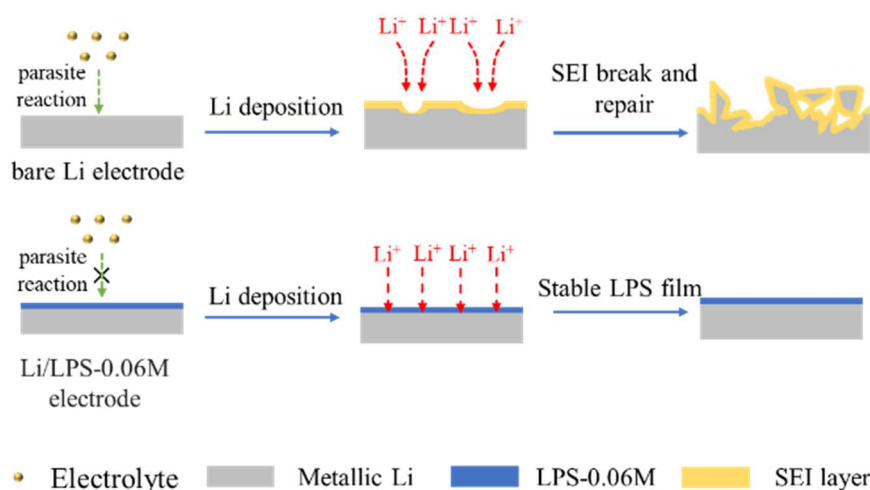


Figure 4. (a) S 2p, (b) P 2p, (c) Li 1s, (d) N 1s and (e) F 1s XPS spectra and the fitting results of the bare Li and Li/LPS-0.06M electrodes after 500 h cycling at  $1 \text{ mA cm}^{-2}$  and  $1 \text{ mAh cm}^{-2}$ .



Schematic 2. Schematic of the bare Li and the Li/LPS-0.06M electrodes during the Li stripping and plating process.

## Li-S and Li-LFP battery test

To test the practical application, the Li/LPS-0.06M electrode and bare Li were evaluated in Li-S full batteries. When the battery is operated at a rate of 0.2 C, the initial capacity of the Li/LPS-0.06M electrode is 1270 mAh g<sup>-1</sup>, while the initial capacity of the bare lithium electrode is only 1090 mAh g<sup>-1</sup> (Figure S13a). In Figure 5a, when the current density is increased to 1 C, the battery with the Li/LPS-0.06M anode has an initial discharge capacity of 910 mAh g<sup>-1</sup>, which is 1.2 times higher than that of 750 mAh g<sup>-1</sup> with the bare Li anode. Remarkably, from the 240<sup>th</sup> cycle to the 800<sup>th</sup> cycle. The capacity of the battery with the Li/LPS-0.06M anode first increases, reaching its maximal capacity at the 576<sup>th</sup> cycle, and then decreases. By comparing the discharge curves at the 320<sup>th</sup> cycle and 640<sup>th</sup> cycle in Figure 5c, it can be observed that the latter

has a longer and flatter second discharge plateau, indicating that the increased capacity is mainly attributed to the more thorough conversion of the low-order polysulfides to  $\text{Li}_2\text{S}/\text{Li}_2\text{S}_2$ . According to relevant literature reports,<sup>46,47</sup> this phenomenon of abnormal capacity increase can be explained by the activation of the S@C cathode during high-rate cycling. During the activation of the S@C cathode, the capacity will increase to a certain extent. After the S@C cathode is fully activated, the capacity will normally decay. The abnormal trend of cycling performance results in a very low-capacity loss at the 800<sup>th</sup> cycle ( $551 \text{ mAh g}^{-1}$ ) in comparison with that at the 240<sup>th</sup> cycle ( $564 \text{ mAh g}^{-1}$ ). The average capacity decay rate from 240<sup>th</sup> to 800<sup>th</sup> cycle is only 0.004%/cycle. In contrast, the capacity of the Li-S battery with the bare Li anode begins decaying rapidly after the 267<sup>th</sup> cycle, and only  $346 \text{ mAh g}^{-1}$  are left after the 800<sup>th</sup> cycle. Additionally, the second discharge plateau of the battery with the Li/LPS-0.06M anode well keeps at 2.0 V during the long-term cycling (Figure 5b), while the one with the bare Li anode decreases from 2.0 V to 1.96 V after 640 cycles (Figure 5c). Figures S13b and c show the charge–discharge profiles of the Li-S batteries with the bare Li anode and Li/LPS-0.06M anode, at a 0.2 C rate. Similarly, the battery with the Li/LPS-0.06M anode exhibits smaller potential polarization and higher specific capacity than those of the battery with the bare Li anode, at a low current density (0.2 C). During standing or

discharging of the Li-S cells, the long-chain polysulfide formed in the cathode diffuses to the surface of the Li anode and is reduced to short-chain polysulfide. Then the short-chain polysulfide moves back to the cathode and is oxidized to long-chain polysulfide.<sup>24</sup> Such reactions continue to proceed in the batteries, reducing the full utilization of active materials and accelerating the capacity decay. As mentioned above, the Li<sub>3</sub>PS<sub>4</sub> artificial SEI layer suppresses the parasitic reactions which include the reactions between the polysulfides and the lithium anode. Therefore, the Li-S batteries with the Li<sub>3</sub>PS<sub>4</sub>-protected Li anode have better capacity retention than those with the bare Li anode.

Besides the capacity retention, the Li<sub>3</sub>PS<sub>4</sub> artificial SEI layer can also improve the rate performance of the Li-S batteries. As shown in Figure 5d, when operating at a 2 C rate, the battery capacity with a bare Li anode drastically decreases to 175 mAh g<sup>-1</sup>, while the battery capacity with a Li/LPS-0.06M anode remains at 682 mAh g<sup>-1</sup>. Comparing the 2 C galvanostatic charge-discharge curves of the two batteries, it can be seen that the one with the bare Li anode shows a much larger overpotential than the one with the Li/LPS-0.06M anode (Figure 5e). A major factor that limits the high-rate performance of the battery with liquid electrolytes is the concentration polarization.<sup>31</sup> Increasing the Li<sup>+</sup> transfer number by substituting liquid electrolyte with solid electrolyte has been demonstrated to be an effective strategy to alleviate the

concentration polarization.<sup>48</sup> In this case, the  $\text{Li}_3\text{PS}_4$  artificial SEI layer increases the local  $\text{Li}^+$  transfer number near the Li anode, where the concentration polarization is the most severe. This helps to lower the overpotential of the batteries when cycling at a high current density.

The  $\text{Li}_3\text{PS}_4$ -protected Li anode is also applied in Li-LFP batteries, to demonstrate the adaptability of this artificial SEI layer for the ester-based electrolytes. The cycling performance of the Li-LFP battery with the Li/LPS-0.06M anode and bare Li anode at 1 C is shown in Figures 6a–c. It can be seen that the capacity of the Li/LPS-0.06M/LFP battery decreased by about 36% during the first 145 cycles, while the capacity of the bare Li/LFP battery decreased by as high as 60%. Moreover, a soft short circuit occurs in the bare Li/LFP battery after 100 cycles, leading to a sharp drop in the coulombic efficiency. In contrast, the coulombic efficiency of the Li/LPS-0.06M/LFP battery can stabilize at about 98% over 145 cycles. The morphology of the protected Li anode and the bare Li anode after 145 cycles at 1 C are characterized by SEM (Figure S14). It can be clearly seen that the surface of the cycled bare Li anode presents a dendritic appearance, indicating that the corrosion reaction and powdering are serious. Generally, the formation of dendritic Li causes excessive volume expansion during the lithium deposition process, increases the charge transfer resistance, and leads to low lithium

utilization and failure of the battery.<sup>15, 49</sup> On the contrary, the surface of the  $\text{Li}_3\text{PS}_4$ -protected Li anode is still smooth after 145 cycles, corresponding with the stable coulombic efficiency of the battery. As well known, different from the ether-based electrolyte, the ester-based electrolyte (1.0 M  $\text{LiPF}_6$  in EC/DEC, 50–50 vol.%) used for Li/LPS batteries cannot spontaneously form stable SEI with the Li anode, so the corrosion of the Li anode is more serious.<sup>50</sup> The results show that the  $\text{Li}_3\text{PS}_4$  artificial SEI layer can effectively suppress the formation of an unstable SEI layer between the Li anode and the ester-based electrolyte, so that the Li/LPS-0.06M/LFP batteries can operate stably.

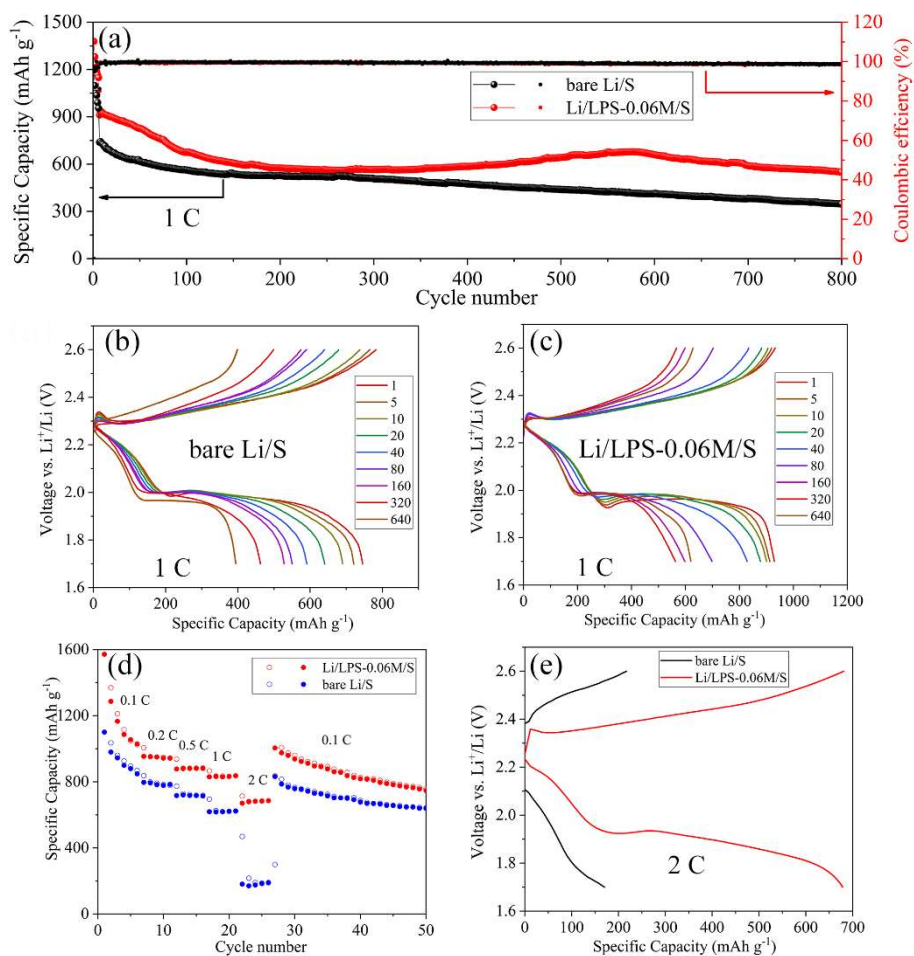


Figure 5. Electrochemical performance of the Li/S batteries with the Li/LPS-0.06M and bare Li anode. (a) Discharge capacity and coulombic efficiency at 1 C. Charge–discharge profiles at 1 C of (b) the bare Li/S and (c) Li/LPS-0.06M/S batteries. (d) Rate performance of the Li/LPS-0.06M/S and bare Li/S batteries; (e) Charge–discharge profiles at 2 C of the bare Li/S and Li/LPS-0.06M/S batteries. (1 C = 1675 mA g<sup>-1</sup>)

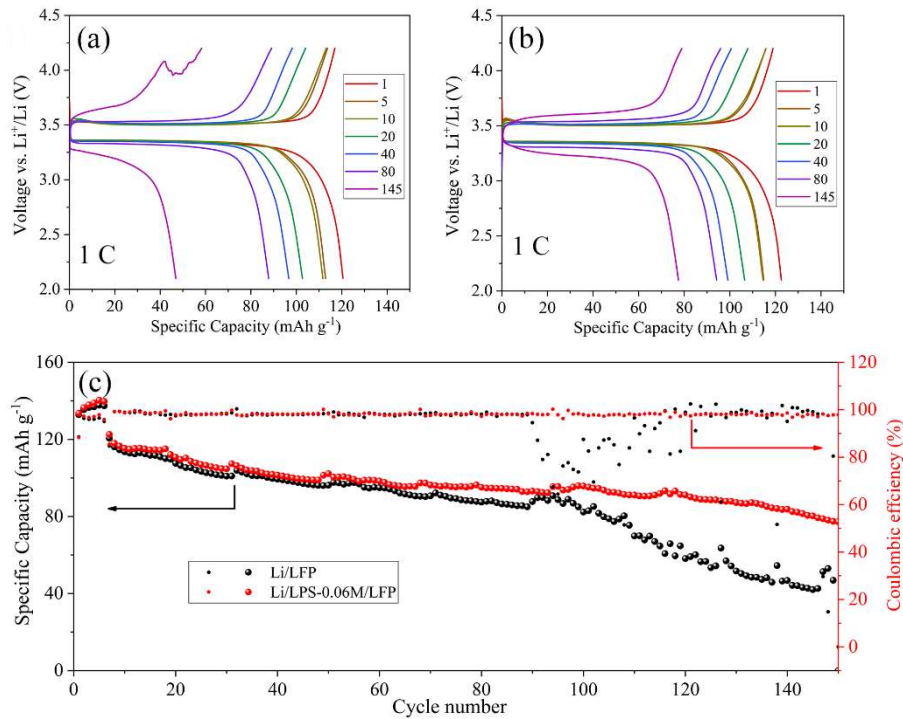


Figure 6. Electrochemical performance of the Li/LFP batteries with the bare Li and Li/LPS-0.06M anode. Charge–discharge profiles of (a) the bare Li/LFP and (b) Li/LPS-0.06M/LFP cells. (c) Discharge capacity and corresponding coulombic efficiency at 1 C. (1 C = 170 mA g<sup>-1</sup>)

## CONCLUSIONS

In this work, 650-nm-thick high-purity Li<sub>3</sub>PS<sub>4</sub> film is directly spin-coated onto the lithium electrode with a lithium-compatible Li<sub>3</sub>PS<sub>4</sub> sol, to serve as an artificial SEI layer. The modification of the lithium electrodes by Li<sub>3</sub>PS<sub>4</sub> limits the parasitic reactions between Li and the organic electrolyte, makes the Li-ion flux uniform, and stabilizes the SEI layer to inhibit Li dendritic growth. As a result, the lithium symmetrical cells with Li<sub>3</sub>PS<sub>4</sub>-modified lithium electrodes can be cycled stably for 800 h at 1 mA cm<sup>-2</sup>. Using the Li<sub>3</sub>PS<sub>4</sub>-modified lithium anode, the Li-S full battery exhibits an initial

capacity of 910 mAh g<sup>-1</sup>, and a low-capacity decay rate of 0.004% per cycle from 240<sup>th</sup> to 800<sup>th</sup> cycles at 1 C. In addition, the Li<sub>3</sub>PS<sub>4</sub> layer significantly enhances the stability of the lithium anode in ester-based electrolytes, so the Li-LiFePO<sub>4</sub> battery with an active material loading of 11.5 mg cm<sup>-2</sup> show stable operation over 145 cycles at 1 C. These results demonstrate that with the spin-coating route developed in this work, the structure of the sulfide-electrolyte-based artificial SEI layer can be well controlled, so that the spin-coated SEI layer effectively improves the stability of the lithium electrodes.

## **ASSOCIATED CONTENT**

### **\*S1 Supporting Information**

Additional Figures S1–S14: SEM images of Li<sub>2</sub>S nanoparticles, Li<sub>3</sub>PS<sub>4</sub> nanoparticles and photograph of as-prepared Li<sub>3</sub>PS<sub>4</sub> sol; EDS spectrum of the Li/LPS-0.06M electrode; morphologies and electrochemical performance of Li/LPS-0.1M, Li/LPS-0.08M, Li/LPS-0.04M and Li/LPS-0.02M symmetric cells; EIS test of the bare Li and Li/LPS-0.06M symmetric cell after 10 cycles; electrochemical performance and SEM of the Li/LPS-0.06M and the bare Li anodes; additional Tables S1–S3: elemental analysis of the Li/LPS-0.06M electrode; fitting the EIS test; comparison of the Li symmetrical batteries with sulfurized SEI and other SEI strategies.

### **Author Contributions**

**Hongjiao Wang:** *Conceptualization, Methodology, Writing-Original Draft.*

**Lilin Wu and Bai Xue:** *Validation, Investigation and Data curation.*

**Fang Wang, Zhongkuan Luo, Xianghua Zhang and Laurent Calvez:**

*Formal analysis, Software, Visualization and Writing-Review & Editing.*

**Ping Fan and Bo Fan:** *Resources, Supervision and Funding acquisition.*

## Notes

There are no conflicts of interest to declare.

## ACKNOWLEDGMENTS

The work is financially supported by the National Natural Science Foundation of China (51702216), the Natural Science Foundation of Guangdong Province (2021A1515011725/ 2020A1515011430), the Stable Support Plan for Shenzhen Higher Education Institutions (20200811211215001) and the Shenzhen Science and Technology Foundation (JCYJ20210324095808023).

## REFERENCES

- (1) Chen, Y.; Yue, M.; Liu, C.; Zhang, H.; Yu, Y.; Li, X.; Zhang, H., Long Cycle Life Lithium Metal Batteries Enabled with Upright Lithium Anode. *Adv. Funct. Mater.* **2019**, *29*, article no. 1806752.
- (2) Fan, J.; Luo, Y.; Jiang, K.; Wang, C., Protection of Lithium Anodes by Fibrous Silica Nanospheres. *RSC Advances* **2020**, *10*, 3145-3152.
- (3) Gu, J.; Shen, C.; Fang, Z.; Yu, J.; Zheng, Y.; Tian, Z.; Shao, L.; Li, X.; Xie, K., Toward High-Performance Li Metal Anode via Difunctional Protecting Layer. *Front*

*Chem* **2019**, *7*, article no. 572.

(4) Hou, G.; Ci, C.; Guo, H.; Zhang, X.; Sun, Q.; Cheng, J.; Salpekar, D.; Ai, Q.; Chen, L.; Puthirath, A. B.; Kato, K.; Pardo, S. C.; Vajtai, R.; Babu, G.; Ci, L.; Ajayan, P. M., Facile Construction of a Hybrid Artificial Protective Layer for Stable Lithium Metal Anode. *Chem. Eng. J.* **2020**, *391*, article no. 123542.

(5) Lee, S. H.; Hwang, J. Y.; Ming, J.; Kim, H.; Jung, H. G.; Sun, Y. K., Long-Lasting Solid Electrolyte Interphase for Stable Li-Metal Batteries. *ACS Energy Lett.* **2021**, *6*, 2153-2161.

(6) Palacin, M. R.; de Guibert, A., Why do Batteries Fail? *Science* **2016**, *351*, article no. 1253292.

(7) Wang, Q.; Liu, B.; Shen, Y.; Wu, J.; Zhao, Z.; Zhong, C.; Hu, W., Confronting the Challenges in Lithium Anodes for Lithium Metal Batteries. *Adv Sci* **2021**, *8*, article no. e2101111.

(8) Wang, Z.; Wang, Y.; Wu, C.; Pang, W. K.; Mao, J.; Guo, Z., Constructing Nitrided Interfaces for Stabilizing Li Metal Electrodes in Liquid Electrolytes. *Chem Sci* **2021**, *12*, 8945-8966.

(9) Lin, D.; Liu, Y.; Cui, Y., Reviving the Lithium Metal Anode for High-energy Batteries. *Nat Nanotechnol* **2017**, *12*, 194-206.

(10) Miao, R. R.; Yang, J.; Feng, X. J.; Jia, H.; Wang, J. L.; Nuli, Y. N., Novel Dual-salts Electrolyte Solution for Dendrite-free Lithium-metal Based Rechargeable Batteries with High Cycle Reversibility. *J. Power Sources* **2014**, *271*, 291-297.

(11) Zheng, J. M.; Engelhard, M. H.; Mei, D. H.; Jiao, S. H.; Polzin, B. J.; Zhang, J. G.; Xu, W., Electrolyte Additive Enabled Fast Charging and Stable Cycling Lithium Metal Batteries. *Nat. Energy* **2017**, *2*, 1-8.

(12) Zhang, X. Q.; Chen, X.; Cheng, X. B.; Li, B. Q.; Shen, X.; Yan, C.; Huang, J. Q.; Zhang, Q., Highly Stable Lithium Metal Batteries Enabled by Regulating the Solvation of Lithium Ions in Nonaqueous Electrolytes. *Angew. Chem. Int. Ed. Engl.* **2018**, *57*, 5301-5305.

(13) Cheng, X.; Yan, C.; Peng, H.; Huang, J.; Yang, S.; Zhang, Q., Sulfurized Solid Electrolyte Interphases with a Rapid Li<sup>+</sup> Diffusion on Dendrite-free Li Metal Anodes. *Energy Storage Mater.* **2018**, *10*, 199-205.

(14) Liu, Y.; Lin, D.; Yuen, P. Y.; Liu, K.; Xie, J.; Dauskardt, R. H.; Cui, Y., An Artificial Solid Electrolyte Interphase with High Li<sup>-</sup> ion Conductivity, Mechanical Strength, and Flexibility for Stable Lithium Metal Anodes. *Adv. Mater.* **2017**, *29*, article no. 1605531.

(15) Liu, T.; Hu, Q.; Li, X.; Tan, L.; Yan, G.; Wang, Z.; Guo, H.; Liu, Y.; Wu, Y.; Wang, J., Lithiophilic Ag/Li Composite Anodes via a Spontaneous Reaction for Li Nucleation

- with a Reduced Barrier. *J. Mater. Chem. A* **2019**, *7*, 20911-20918.
- (16) Yan, X.; Zhang, H.; Huang, M.; Qu, M.; Wei, Z., Self-Formed Protection Layer on a 3D Lithium Metal Anode for Ultrastable Lithium-Sulfur Batteries. *ChemSusChem* **2019**, *12*, 2263-2270.
- (17) Zhang, H.; Ju, S.; Xia, G.; Sun, D.; Yu, X., Dendrite - Free Li - Metal Anode Enabled by Dendritic Structure. *Adv. Funct. Mater.* **2021**, *31*, article no. 2009712.
- (18) Luo, Z.; Qiu, X.; Liu, C.; Li, S.; Wang, C.; Zou, G.; Hou, H.; Ji, X., Interfacial Challenges Towards Stable Li Metal Anode. *Nano Energy* **2021**, *79*, article no. 105507.
- (19) Hu, A.; Chen, W.; Du, X.; Hu, Y.; Lei, T.; Wang, H.; Xue, L.; Li, Y.; Sun, H.; Yan, Y.; Long, J.; Shu, C.; Zhu, J.; Li, B.; Wang, X.; Xiong, J., An Artificial Hybrid Interphase for an Ultrahigh-rate and Practical Lithium Metal Anode. *Energy Environ. Sci.* **2021**, *14*, 4115-4124.
- (20) Zhang, Y.; Sun, C., Composite Lithium Protective Layer Formed In Situ for Stable Lithium Metal Batteries. *ACS Appl. Mater. Interfaces* **2021**, *13*, 12099-12105.
- (21) Li, N. W.; Yin, Y. X.; Yang, C. P.; Guo, Y. G., An Artificial Solid Electrolyte Interphase Layer for Stable Lithium Metal Anodes. *Adv. Mater.* **2016**, *28*, 1853-1858.
- (22) Pang, Q.; Liang, X.; Shyamsunder, A.; Nazar, L. F., An In Vivo Formed Solid Electrolyte Surface Layer Enables Stable Plating of Li Metal. *Joule* **2017**, *1*, 871-886.
- (23) Liang, J.; Li, X.; Zhao, Y.; Goncharova, L. V.; Wang, G.; Adair, K. R.; Wang, C.; Li, R.; Zhu, Y.; Qian, Y.; Zhang, L.; Yang, R.; Lu, S.; Sun, X., In Situ Li<sub>3</sub>PS<sub>4</sub> Solid-State Electrolyte Protection Layers for Superior Long-Life and High-Rate Lithium-Metal Anodes. *Adv. Mater.* **2018**, *30*, article no. e1804684.
- (24) Li, M.; Liu, X.; Li, Q.; Jin, Z.; Wang, W.; Wang, A.; Huang, Y.; Yang, Y., P<sub>4</sub>S<sub>10</sub> Modified Lithium Anode for Enhanced Performance of Lithium-sulfur Batteries. *J. Energy. Chem.* **2020**, *41*, 27-33.
- (25) Liu, Z.; Fu, W.; Payzant, E. A.; Yu, X.; Wu, Z.; Dudney, N. J.; Kiggans, J.; Hong, K.; Rondinone, A. J.; Liang, C., Anomalous High Ionic Conductivity of Nanoporous Beta-Li<sub>3</sub>PS<sub>4</sub>. *J. Am. Chem. Soc.* **2013**, *135*, 975-978.
- (26) Fan, B.; Zhang, Q.; Luo, Z.; Zhang, X.; Ma, H.; Fan, P.; Xue, B., Influence of precipitate/supernatant ratio during liquid-phase synthesis of solid electrolyte Li<sub>7</sub>P<sub>3</sub>S<sub>11</sub>. *Solid State Ionics* **2019**, *343*, article no. 115073.
- (27) Hayashi, A.; Minami, K.; Ujiie, S.; Tatsumisago, M., Preparation and Ionic Conductivity of Li<sub>7</sub>P<sub>3</sub>S<sub>11</sub>-z Glass-ceramic Electrolytes. *J. Non-Cryst. Solids* **2010**, *356*, 2670-2673.
- (28) Wood, K. N.; Kazyak, E.; Chadwick, A. F.; Chen, K. H.; Zhang, J. G.; Thornton, K.; Dasgupta, N. P., Dendrites and Pits: Untangling the Complex Behavior of Lithium

- Metal Anodes through Operando Video Microscopy. *ACS Cent Sci* **2016**, *2*, 790-801.
- (29) Chen, K.-H.; Wood, K. N.; Kazyak, E.; LePage, W. S.; Davis, A. L.; Sanchez, A. J.; Dasgupta, N. P., Dead Lithium: Mass Transport Effects on Voltage, Capacity, and Failure of Lithium Metal Anodes. *J. Mater. Chem. A* **2017**, *5*, 11671-11681.
- (30) Gunnarsdottir, A. B.; Amanchukwu, C. V.; Menkin, S.; Grey, C. P., Noninvasive In Situ NMR Study of "Dead Lithium" Formation and Lithium Corrosion in Full-Cell Lithium Metal Batteries. *J. Am. Chem. Soc.* **2020**, *142*, 20814-20827.
- (31) Bai, P.; Li, J.; Brushett, F. R.; Bazant, M. Z., Transition of Lithium Growth Mechanisms in Liquid Electrolytes. *Energy Environ. Sci.* **2016**, *9*, 3221-3229.
- (32) Ma, G.; Wen, Z.; Wang, Q.; Shen, C.; Jin, J.; Wu, X., Enhanced Cycle Performance of a Li-S Battery Based on a Protected Lithium Anode. *J. Mater. Chem. A* **2014**, *2*, 19355-19359.
- (33) Fan, B.; Xu, Y.; Ma, R.; Luo, Z.; Wang, F.; Zhang, X.; Ma, H.; Fan, P.; Xue, B.; Han, W., Will Sulfide Electrolytes be Suitable Candidates for Constructing a Stable Solid/Liquid Electrolyte Interface? *ACS Appl. Mater. Interfaces* **2020**, *12*, 52845-52856.
- (34) Wenzel, S.; Weber, D. A.; Leichtweiss, T.; Busche, M. R.; Sann, J.; Janek, J., Interphase Formation and Degradation of Charge Transfer Kinetics Between a Lithium Metal Anode and Highly Crystalline  $\text{Li}_7\text{P}_3\text{S}_{11}$  Solid Electrolyte. *Solid State Ionics* **2016**, *286*, 24-33.
- (35) Lu, Y.; Gu, S.; Hong, X.; Rui, K.; Huang, X.; Jin, J.; Chen, C.; Yang, J.; Wen, Z., Pre-modified  $\text{Li}_3\text{PS}_4$  Based Interphase for Lithium Anode Towards High-performance Li-S Battery. *Energy Storage Mater.* **2018**, *11*, 16-23.
- (36) Aurbach, D.; Pollak, E.; Elazari, R.; Salitra, G.; Kelley, C. S.; Affinito, J., On the Surface Chemical Aspects of Very High Energy Density, Rechargeable Li-Sulfur Batteries. *J. Electrochem. Soc.* **2009**, *156*, article no. A694.
- (37) Jeong, J.; Lee, J.; Kim, J.; Chun, J.; Kang, D.; Han, S. M.; Jo, C.; Lee, J., A Biopolymer-based Functional Separator for Stable Li Metal Batteries with an Additive-free Commercial Electrolyte. *J. Mater. Chem. A* **2021**, *9*, 7774-7781.
- (38) Jin, D.; Roh, Y.; Jo, T.; Ryou, M. H.; Lee, H.; Lee, Y. M., Robust Cycling of Ultrathin Li Metal Enabled by Nitrate - Preplanted Li Powder Composite. *Adv. Energy Mater.* **2021**, *11*, article no. 2003769.
- (39) Kang, H.; Song, M.; Yang, M.; Lee, J. W., Lithium Metal Anode with Lithium Borate Layer for Enhanced Cycling Stability of Lithium Metal Batteries. *J. Power Sources* **2021**, *485*, article no. 229286.
- (40) Fu, L.; Wang, X.; Wang, L.; Wan, M.; Li, Y.; Cai, Z.; Tan, Y.; Li, G.; Zhan, R.; Seh, Z. W.; Sun, Y., A Salt - in - Metal Anode: Stabilizing the Solid Electrolyte Interphase

- to Enable Prolonged Battery Cycling. *Adv. Funct. Mater.* **2021**, *31*, article no. 2010602.
- (41) Xiong, S.; Xie, K.; Diao, Y.; Hong, X., Properties of Surface Film on Lithium Anode with LiNO<sub>3</sub> as Lithium Salt in Electrolyte Solution for Lithium–sulfur Batteries. *Electrochim. Acta* **2012**, *83*, 78-86.
- (42) Tang, W.; Yin, X.; Kang, S.; Chen, Z.; Tian, B.; Teo, S. L.; Wang, X.; Chi, X.; Loh, K. P.; Lee, H. W.; Zheng, G. W., Lithium Silicide Surface Enrichment: A Solution to Lithium Metal Battery. *Adv. Mater.* **2018**, *30*, article no. e1801745.
- (43) Jie, J.; Liu, Y.; Cong, L.; Zhang, B.; Lu, W.; Zhang, X.; Liu, J.; Xie, H.; Sun, L., High-performance PVDF-HFP Based Gel Polymer Electrolyte with a Safe Solvent in Li Metal Polymer Battery. *J. Energy. Chem.* **2020**, *49*, 80-88.
- (44) Yang, T.; Sun, Y.; Qian, T.; Liu, J.; Liu, X.; Rosei, F.; Yan, C., Lithium Dendrite Inhibition via 3D Porous Lithium Metal Anode Accompanied by Inherent SEI Layer. *Energy Storage Mater.* **2020**, *26*, 385-390.
- (45) Xia, S.; Zhang, X.; Liang, C.; Yu, Y.; Liu, W., Stabilized Lithium Metal Anode by an Efficient Coating for High-performance Li–S Batteries. *Energy Storage Mater.* **2020**, *24*, 329-335.
- (46) Cheng, J.; Zhao, D.; Fan, L.; Wu, X.; Wang, M.; Zhang, N.; Sun, K., Ultra-high rate Li–S batteries based on a novel conductive Ni<sub>2</sub>P yolk–shell material as the host for the S cathode. *J. Mater. Chem. A* **2017**, *5*, 14519-14524.
- (47) Xu, Y. H.; Zhang, Q. F.; Fan, B.; Xue, B.; Chen, H. J.; Zhang, X. H.; Luo, Z. K.; Wang, F.; Le Coq, D.; Calvez, L.; Ma, H. L.; Fan, P., An Extremely High Rate Li–S Battery with Hybrid Electrolyte. *J. Alloys Compd.* **2020**, *845*, article no. 156261.
- (48) Kato, Y.; Hori, S.; Saito, T.; Suzuki, K.; Hirayama, M.; Mitsui, A.; Yonemura, M.; Iba, H.; Kanno, R., High-power All-solid-state Batteries Using Sulfide Superionic Conductors. *Nat. Energy* **2016**, *1*, 1-7.
- (49) Yang, X.; Gao, X.; Zhao, C.; Sun, Q.; Zhao, Y.; Adair, K.; Luo, J.; Lin, X.; Liang, J.; Huang, H.; Zhang, L.; Lu, S.; Li, R.; Sun, X., Suppressed Dendrite Formation Realized by Selective Li Deposition in All-solid-state Lithium Batteries. *Energy Storage Mater.* **2020**, *27*, 198-204.
- (50) Qiu, H.; Tang, T.; Asif, M.; Li, W.; Zhang, T.; Hou, Y., Stable Lithium Metal Anode Enabled by Lithium Metal Partial Alloying. *Nano Energy* **2019**, *65*, article no. 103989.

By spin-coating of a  $\text{Li}_3\text{PS}_4$  sol, a  $\text{Li}_3\text{PS}_4$  artificial SEI layer is prepared on the lithium electrode, which uniformizes the  $\text{Li}^+$  flux and isolates the parasite reaction. The modified electrode cycles for 800 h at  $1 \text{ mA cm}^{-2}$ .

